Arch. Metall. Mater. **67** (2022), 2, 397-403

DOI: https://doi.org/10.24425/amm.2022.137770

AMIR TOOFANI SHAHRAKI[1], HEYDAR ALI SHAFIEI GOL[1*],
SALIMEH KIMIAGAR[2], NASER ZARE DEHNAVI[1]

ENHANCEMENT OF THERMOELECTRIC EFFICIENCY AND OPTICAL PROPERTIES OF HYDROGEN ABSORPTION IN SIC:MN NANOTUBE

The effects of hydrogen absorption and manganese substitution on structural, electronic, optical, and thermoelectric properties of silicon-carbon nanotubes (SiCNT) are studied using the density functional theory and the GGA approximation. An examination of the PDOS curves and the electronic band structure showed that the Mn substitution leads to an increase in magnetic anisotropy and the occurrence of semi-metallic behavior and that the hydrogen absorption shifts the band gap toward the lower energies. A study of these nanostructures' thermoelectric behavior reveals that the H absorption leads to a significant escalation in the figure of merit of the SiCNT to about 1.6 in the room temperature range. The effects of the H absorption on this nanotube's optical properties, including the dielectric functions and its absorption spectra, are also investigated.

Keywords: DFT; SiC:Mn-H NT; electronic property; thermometric; optical property

1. Introduction

Achieving high thermoelectric (TE) performance is one of the challenges in studying TE materials. TE performance can be measured through the dimensionless figure of merit (ZT), where T is the absolute temperature, S is the Seebeck coefficient, σ is the electrical conductivity, and k is the thermal conductivity, including the share of the lattice and the electron ($K = K_{el} + K_{latt}$) [1,2]. One way to improve the thermoelectric efficiency of materials and increase the amount of ZT is to create nanostructures. In 1993, Hicks and Dresselhaus predicted that the amount of ZT for small size nanostructures (1D and 2D) would increase significantly, possibly due to quantum confinement and surface phonon scattering [3,4]. This idea has widely been studied in theoretical and experimental fields and demonstrated an increase in TE performance for different materials. Among the one-dimensional materials, carbon nanotubes (CNTs) have shown significant electronic transport properties [5-8], which are used as additives to improve the TE performance of organic compounds [9,10].

In this regard, silicon-carbon (SiC) is a ceramic that has been widely used in high-temperature thermoelectric structures. Due to its high resistance to heat and oxidation, this particular compound has shown a high amount of thermal conductivity (about 120 W/mK), which results in a small amount of ZT [11-17]. Therefore, searching the achievement of higher ZT and reducing thermal conductivity, methods such as making nanotubes, nanoparticles, or creating nanowires based on SiC have been widely studied, all of which improve the TE performance compound. For example, the fabrication of SiC nanowires (SiCNWs) has reduced thermal conductivity due to the increase in boundary phonon scattering, which makes nanowire structures a good candidate for TE nanodevices [18-20]. Besides, reports of increased Seebeck levels for SiC nanoparticles have been shown to have significant thermoelectric properties at high temperatures [21-23]. These nanoparticles have a Seebeck coefficient of about 520 μVK^{-1} and a very low thermal conductivity of about 0.6 W/mK compared to suitable traditional TE materials such as Bi2Te3 and PbTe with high Seebeck values of about 170 μVK^{-1} and 370 μVK^{-1} [24-27].

In recent years, SiC Nanotubes (SiCNTs), as other preferred nanostructures, have been extensively studied due to their unique properties such as wide band gap, high atomic binding energy, high electron mobility, high radiation resistance [28-31] and high potential for applications in atomic field emissions [32], nanophase storage devices [33], gas detectors [34]

[1] DEPARTMENT OF PHYSICS, CENTRAL TEHRAN BRANCH, ISLAMIC AZAD UNIVERSITY, TEHRAN, IRAN
[2] NANO RESEARCH LAB(NRL), DEPARTMENT OF PHYSICS, CENTRAL TEHRAN BRANCH, ISLAMIC AZAD UNIVERSITY, TEHRAN, IRAN

* Corresponding author: hshafieigol@yahoo.com

and hydrogen storage [35-38]. Doping has been used as one of the best ways to improve these nanotubes' properties in recent decades [37,39-42]. Accordingly, contamination with acceptor or donor elements of 3A and 4A groups of the periodic table has been significant [43-48]. The study of hydrogen storage in carbon nanotubes (CNTs) doped with metals has been carried out by many groups, the results of which provide the high binding energy of hydrogen compared to the pure CNTs [49-51]. However, there are few reports of hydrogen absorption on SiC nanotubes [36,38,52,53], namely, the research performed on the electronic structure of SiCNT doped with sulfur by R.S. Singh and A. Solanki [37] or the H absorption of the Li-doped SiCNT by Wang et al. [54]. Therefore, in the present study, the electronic and thermoelectric behavior of single-walled (3,0) zigzag SiC nanotubes have been studied under the substitution of manganese's transition metal in its center and then the absorption of H on Mn, that no work has been reported on this discussion so far. Thus, in the first part: Structural features, in the second part: electronic behavior, in the third part: electronic transport, and in the fourth part: Optical properties of SiC nanoparticles doped with Mn and hydrogen absorption in it have been discussed.

2. Computational details

Total energy and electronic structure were calculated using the first principle study of the full-potential (linearized) augmented plane-wave (FP-LAPW) method within the framework of DFT [55,56] and Wien2K code [57]. The generalized gradients approximation (GGA) [58] was considered for exchange-correlation potential term, $R_{mt}K_{max} = 7.5$. The core states are the 1s electrons of C and the 2p electrons of Si and Mn atoms. Along with the nanotube axis, 1×1×10 Monkhorst-pack k-points were considered for the integration of the first Brillouin zone, and the Gmax is selected to 13.5 number. The value of 10Å is considered for the inter-wall distance between adjacent SiCNTs using periodic boundary conditions and supercell approximation to eliminate the tube-tube interactions. The convergence of structural optimization continued until the force applied to each atom was less than 0.01 eV/A. Moreover, this nanotube's electron transport behavior and the effect of hydrogen adsorption are studied using the BoltzTraP code [59] and solving Boltzmann's quasi-classical equations in the temperature range of 200 to 1200 K.

3. Results and discussion

3.1. Structural properties

In order to investigate the hydrogen absorption on the SiC nanotube, the SiC zigzag (3.0) nanotube is firstly optimized by placing the manganese atom in its center and then optimizing it by adding H on Mn. These optimized configurations are shown in Figure 1. The average Si-C bond length, in this case, is about 1.8Å, and the Mn-H bond length after optimization is about 1.5Å, which is similar to other calculations [60]. In Table 1,

TABLE 1

The nanotube diameter D(Å), lattice constants (a, c (Å)), Binding energy (E_b(Ryd)), total magnetic moment $M_{tot}(\mu_B)$, Spin polarization at Fermi level P(%), Static dielectric function (ε(0)) for SiCNT, SiCNT:Mn, SiCNT:Mn-H

	D	a, c	E_b	M_{tot}	P	ε(0)	
						Parallel	Perpendicular
SiCNT	5. 3	20.00, 5.34	–0.521	0.00	0	2.4	1.98
SiCNT:Mn	5.81	37.79, 10.09	–0.479	5.00	100	2.4	2.49
SiCNT: Mn-H	5.83	37.79, 10.09	–0.498	4.90	80	-17.9	2.88

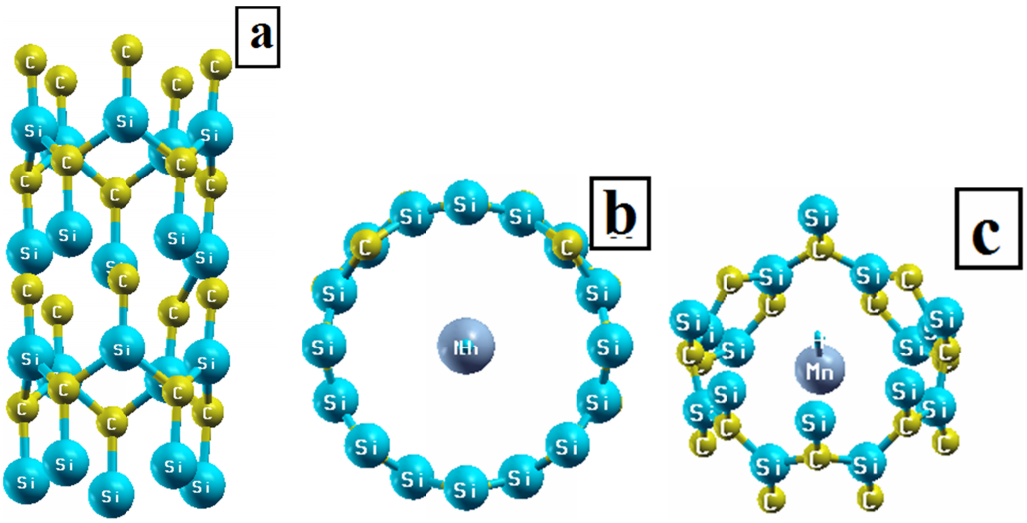

Fig. 1 (a) Pure SiC, (b) Mn absorption, and (c) Mn-H absorption

the amount of binding energy for this system is calculated and presented according to Equation (1) [61].

$$E_b = E_{NT:Mn-H} - E_{NT} - E_{Mn-H} \quad (1)$$

which $E_{NT:Mn-H}$, E_{NT}, and E_{Mn-H} are the total energy values of nanotubes with Mn-H molecule, pure nanotube and Mn-H molecule, respectively. The optimized values of lattice constants and nanotube diameters are also listed in Table 1 for all three cases.

3.2. Effects of hydrogen absorption on electronic behavior of SiC nanotube

From the pure SiCNT electronic structure, a direct band gap of about 1.46 eV is observed in Figure 2(a). From the PDOS curves and the band structure, it is clear that this gap is due to the strong hybridization of Si-3p and C-2p states at the edge of the valance band (VBM) and the conduction band edge (CBM).

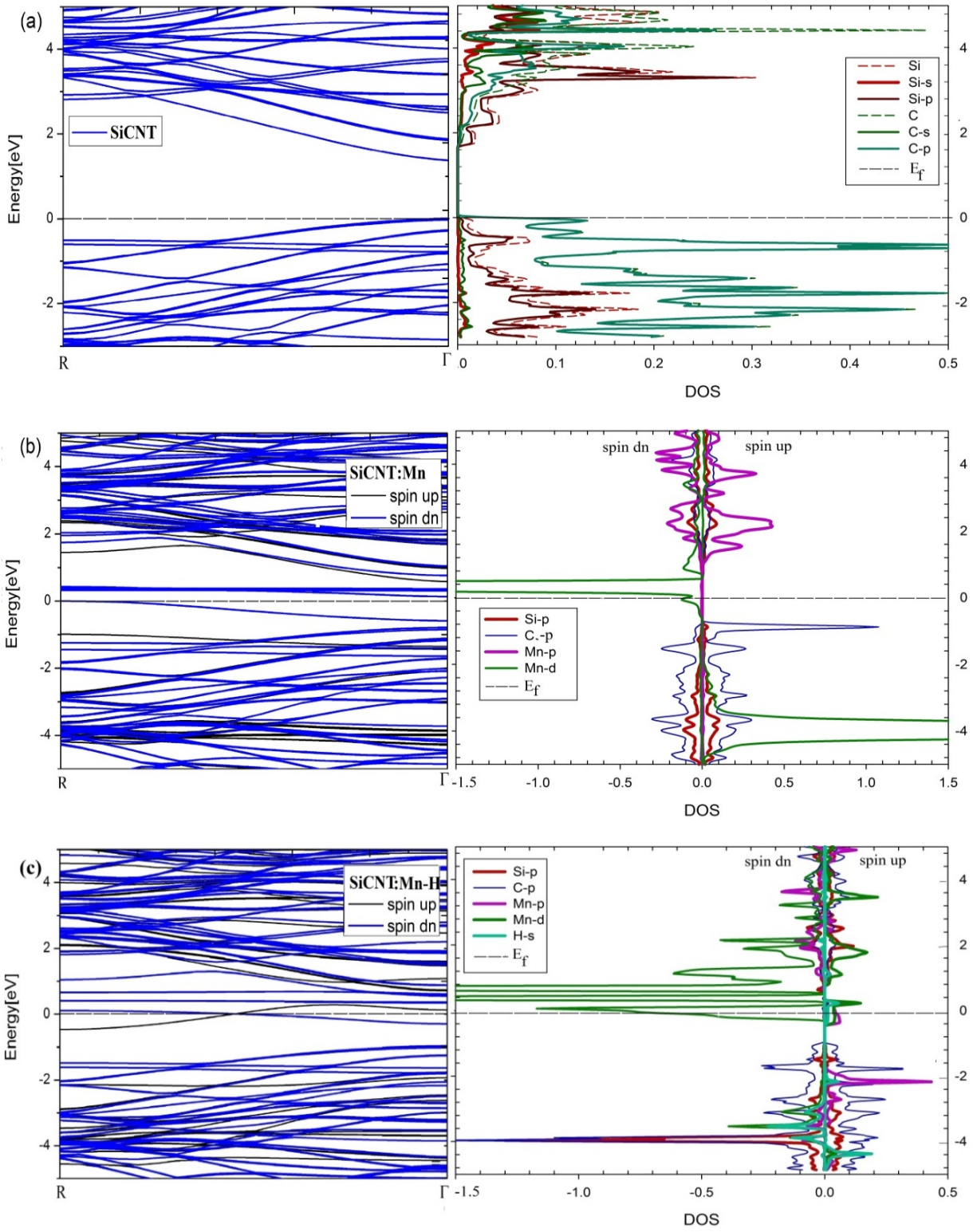

Fig. 2. The bandstructure and DOS of the (a) SiCNT, (b) SiCNT:Mn, (c) SiCNT:Mn-H, for two up and down spins

Most of the densities of states for this structure are due to the same p-orbitals. The magnitude of this structure's magnetic moment is about zero, indicating the non-magnetic behavior and the zero spin polarization for this nanotube. The Fermi level is located just above the valance band, displaying the p-type conductivity behavior. Then, the substitution Mn atom at the center of the nanotube and its effect on electronic behavior has been examined. According to Figure 2(b), it can be observed from the spin-polarized partial density of states curve that the presence of manganese atoms leads to magnetic anisotropy in this structure as in the majority spin, the interactions of the p-states of the Si, Mn, and C atoms cause a direct large band gap of about 1.2 eV and a spin-flip gap of about 0.8 eV at the Fermi level while in the minority spin, metallic behavior is resulted due to the existence of strong Mn-3d states in the Fermi level. In this case, the magnetic moment is about $5\mu_B$, and the spin polarization at the Fermi level is 100%.

In the next step, in Figure 2(c) the effects of hydrogen absorption are illustrated. The results show that placing the H atom on the manganese in the nanotube center has led to a shift in the edge conduction states towards the Fermi level in both spin channels. In spin up, it is seen that the Fermi level is crossed by H-1s, Mn-3d, and Mn-3p states, while in spin down, high-gradient Mn-3d states are replaced at the Fermi level, and the band gap is shifted to lower energies. There is a negative gap of about 0.4 eV 0.6 eV in up and down spin channels, respectively. As can be seen, the presence of these levels at the Fermi level has caused the magnetic moment to be somewhat similar to the previous state, i.e. the Mn substitution, to be about $4.9\mu_B$. Furthermore, there is a spin polarization of 80% due to hydrogen absorption for the SiC nanotube.

As shown in Figure 2, there is a Van Hove singularity at the edge of the maximum valence. Under these conditions, no energy transfer occurs in this point and we see standing waves in this area. But with the entering the Mn impurity, singularity has been eliminated, and the mobility of electrons and holes are increased.

3.3. Thermoelectric properties

The electrical conductivity (σ), Seebeck coefficient (S), power factor (PF), and thermal conductivity of electron contribution (Kel) which are calculated with the GGA approximation are depicted in Figure 3 for the SiC nanotube under manganese substitution and hydrogen absorption in the majority spin where the semiconductor behavior is observed. The Seebeck coefficient, which represents the amount of electrical voltage generated by applying temperature gradient in materials ($-\Delta V/\nabla T$), shows a positive trend with increasing temperature for pure SiCNT in the range of 200 to 1200 K. These positive S values confirm the p-type conductivity for this nanotube, but with the substitution of Mn and after the H absorption, a change in the behavior of Seebeck coefficient can be detected from positive values to negative ones which means changing behavior from p-type conductivity to n-type one. The highest S value occurs of SiCNT:Mn at about 200 K (about –248 μV/K) and then experiences a decreasing trend with increasing temperature, it is shown that SiCNT:Mn has higher S parameter than other cases with electron transportation. The changes in electrical conductivity (σ/τ), considering the relaxation time approximation (τ), show a rising linear trend with increasing temperature for pure SiCNT,

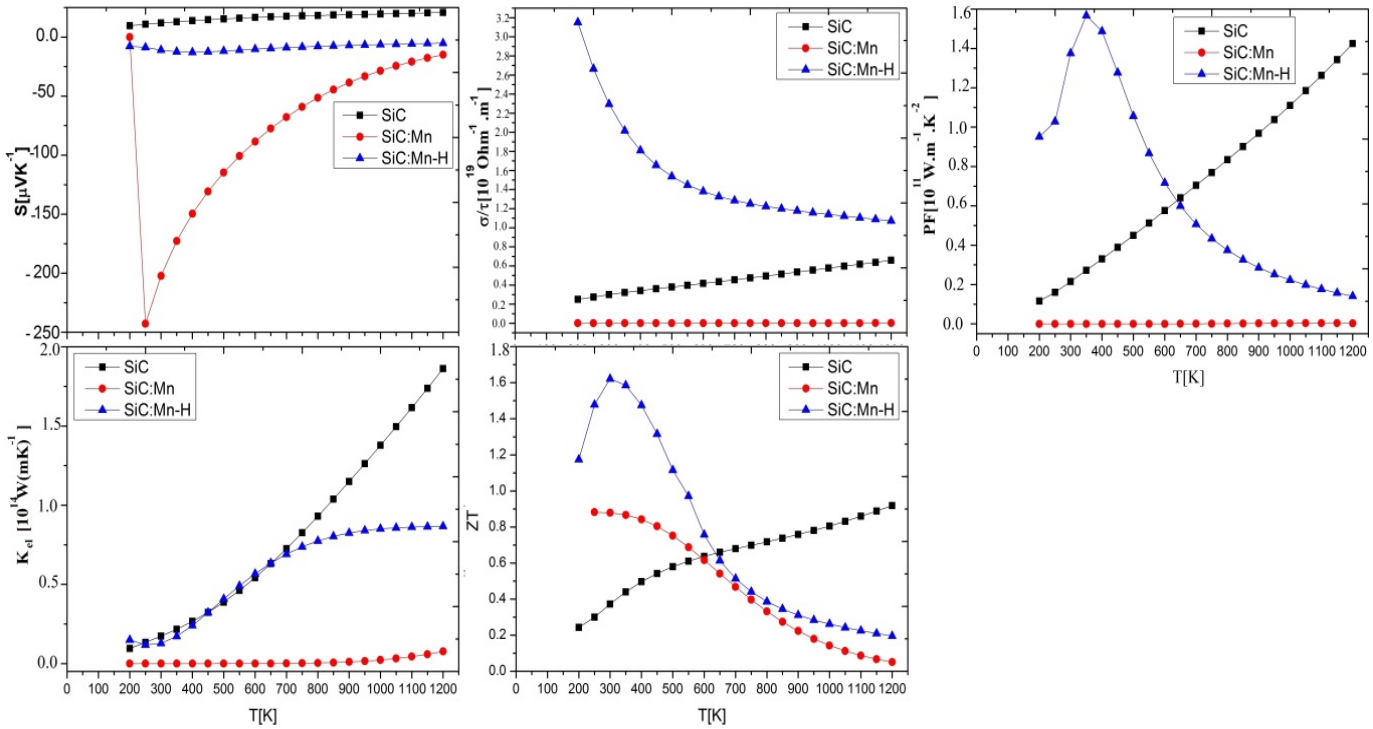

Fig. 3. The S, σ/τ, PF, K_{el}, and ZT curves of the SiCNT, SiCNT:Mn, and SiCNT:Mn-H

whereas after Mn substitution at its center, the value of σ/τ is very small throughout the temperature range and it is close to zero. However, the H absorption leads to a complete reversal of the variations of this parameter, so that after reaching the maximum value at 200 K, a decreasing trend is seen. The K_{el} parameter also shows similar behavior to σ/τ. For pure SiCNT, the K_{el} change trend is positive, and in the Mn substitution mode, little amounts of K_{el} occur.

Temperature changes of the power factor, which is defined as $S^2\sigma/\tau$ is shown in Figure 3. The maximum PF for pure SiCNT at 1200 K is about 1.43 [10^{11} W.m^{-1}.K^{-2}]. With the Mn substitution, the PF value is significantly reduced and then with H absorption, the peak of this quantity at 400 K is about 1.59 [10^{11} W.m^{-1}.K^{-2}] followed by a decrease in PF by increasing T. The great peak PF of the SiCNT:Mn-H in lower temperatures, make it as a suitable candidate for cooling applications, and at increased this parameter at higher temperatures make the SiCNT as a good case for power generator applications. Additionally, the main parameter in determining the thermoelectric performance and electron transport of materials, namely the figure of merit (ZT), is also examined. The results represent that the maximum ZT value for pure SiCNT at about 1200 K is about 0.92. After manganese substitution, the maximum ZT at 300 K is about 0.85. After hydrogen absorption, the highest ZT in the room temperature range is significantly increased compared to the previous two states to reach about 1.6. It is noteworthy that pure SiCNT exhibits good thermoelectric performance at high temperatures whilst under Mn substitution and H absorption, this behavior is transferred to the room temperature range. Therefore, it can be said that pure SiCNT will be suitable for the application of thermoelectric power generation at high temperatures, while under Mn substitution and H absorption, it is an excellent candidate for thermoelectric coolers.

3.4. Optical properties

The SiC nanotube has shown many practical aspects in optical devices [62-65]. A study of the effects of manganese substitution and hydrogen absorption on the optical properties of this nanotube provides the ability to identify the capabilities of this nanostructure. Optical parameters including the dielectric function (ε_1 and ε_2), the electron energy loss function, and the absorption spectra have been drawn in Figure 4 for two directions of parallel to the nanoparticle axis (Parallel) and perpendicular to it (Perpendicular). In Parallel mode, ε_1 demonstrates similar behavior at low energies for SiCNT and SiCNT:Mn. The static values of ε_1 are listed in Table 1. However, with the H absorption, the static value tends to large negative amounts, confirming the electronic structure's metallic behavior. There is no negative value for ε_1 in the entire photon energy range, while Mn's presence resulted in a high dielectric peak at 7.65 eV. The main peak of the SiCNT:Mn-H is at about 2.5eV, and the two ε_1 peaks for SiCNT and SiCNT:Mn in 3.5 eV and 3eV energy, respectively, are all due to electronic transitions between Mn-3d, Mn-3p, Si-3p and C-2p states. The behavior of ε_1 in the perpendicular mode is very similar to Parallel mode, i.e. peaks are in similar positions. However, the static values of 1 for

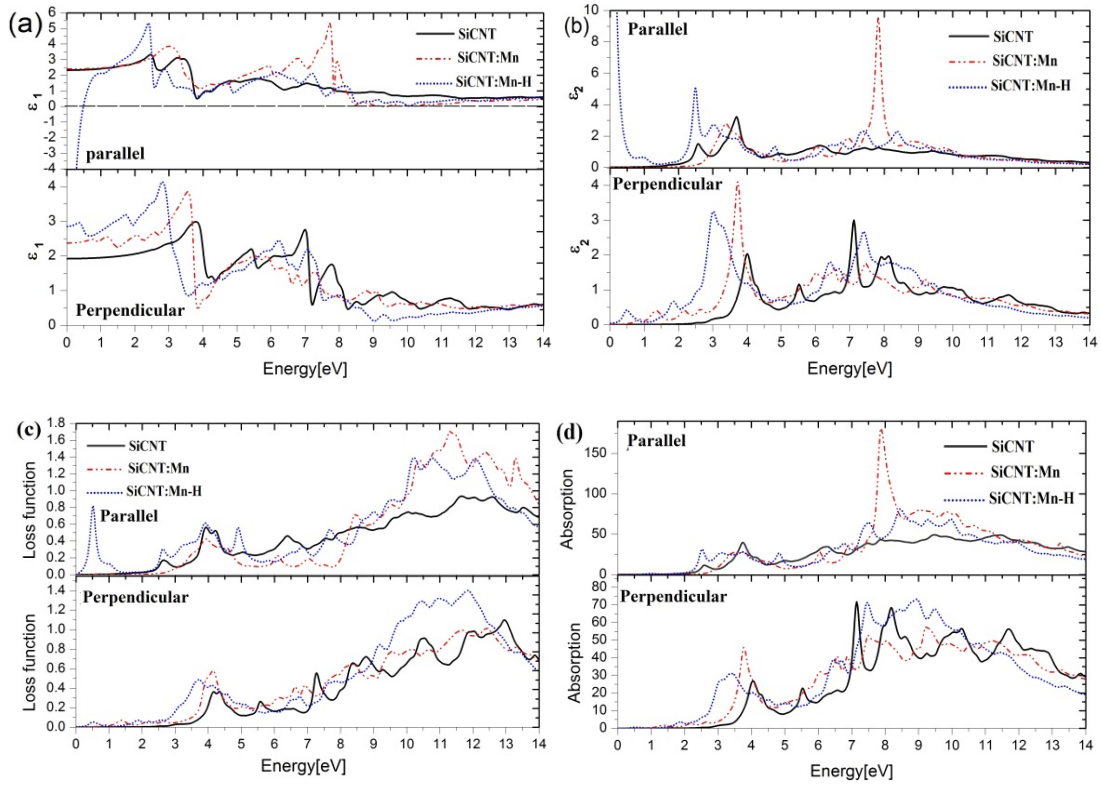

Fig. 4. (a) ε_1, (b) ε_2, (c) Loss function, and (d) Absorption of the SiCNT, SiCNT:Mn, SiCNT:Mn-H

Mn substitution and H adsorption show an increase relative to the pure SiC state. The imaginary part of the dielectric function (ε_2) has a very close relationship with the electronic structure of matter, which is depicted for the two mentioned directions in Figure 4b. Behavioral similarity ε_2 in both parallel and perpendicular directions is very high. The high-intensity peak of SiCNT:Mn-H in the infrared range of Parallel direction referred to its metallic behavior. Noteworthy is the behavioral difference of ε_1 and similarly ε_2 in parallel and perpendicular directions, declaring the optical anisotropy property for these nanotubes.

Another crucial optical parameter is electron energy loss function. Following the diagrams of the imaginary part of the dielectric function, it is clear that in the parallel direction for SiCNT:Mn-H, the peak is at about 0.6 eV energy simultaneously as the root occurrence ε_1 indicates Plasmon intensification for this nanotube. The peaks of the energy loss spectrum in both directions range from 2.5 eV to 14 eV, which, similarly, for all three modes of SiCNT, SiCNT:Mn, and SiCNT:Mn-H all peaks are due to interband transitions. Only the SiCNT:Mn has a peak in the infrared region along the parallel direction and other cases for two directions have no peaks. So, in the SiCNT:Mn case with change the light direction, it can act like an optical switch in the infrared region. Accordingly, anisotropy can be seen in the energy loss spectrum for both directions light radiation directions so that the energy loss spectrum in the perpendicular direction is less intense. In Figure 4d, the optical absorption spectrum for these three nanotube states is calculated and shown. For both directions, no absorption has occurred up to about 2 eV, indicating an optical gap of about 2 volts. The manganese substitution and the H adsorption have led to good absorption at about (2-4 eV) relative to the pure SiCNT state, which in addition to good absorption in the ultraviolet region simultaneously with intraband transitions; the optical absorption spectrum is a significant quantity for photovoltaic cells.

4. Conclusion

The first principle calculations are applied to investigate the structural, electronic, and thermoelectric properties of the (3,0) SiC nanotube under Mn substitution and H absorption. The results demonstrate that the pure SiCNT is a non-magnetic p-type semiconductor with a band gap of about 1.4 eV, and by Mn substitution intensifies magnetic anisotropy, and it exhibits the half-metallic properties so that semiconductor behavior in up spin with a band gap of about 1.2 eV and metallic behavior in down spin. The hydrogen absorption in this nanotube leads to the conduction edge shift toward the Fermi level and the band gap shift toward negative energies. The study of the thermoelectric behavior of this nanotube also displays a significant increase of ZT parameter due to this absorption to about 1.6. The Seebeck coefficient changes show that p-type conductivity in pure SiCNT has changed with manganese substitution and H absorption to n-type conductivity. A study of optical parameters such as dielectric functions, optical absorption spectra and electron energy loss function for this nanotube shows that the presence of hydrogen lead to the occurrence of effective optical absorptions in the visible range, which in addition to good absorption in ultraviolet, it is an effective factor in optoelectronic applications.

REFERENCES

[1] G. Mpourmpakis, G.E. Froudakis, G.P. Lithoxoos, J. Samios, Nano Lett. **6**(8), 1581 (2006).

[2] X. Shi, L. Chen, C. Uher, International Materials Reviews **61** (6), 379 (2016).

[3] L.D. Hicks, M.S. Dresselhaus, Phys. Rev. B 47, 12727 (1993).

[4] C. Giulio, B. Andrea, F. Vincenzo, Phys. Rev. Materials **4**, 075404 (2020).

[5] P.H. Jiang, et. al., Physical Chemistry Chemical Physics **17** (41), 27558 (2015).

[6] C.J. An, H. Kang, H. Song, Y. Jeong, S.Y. Cho, Journal of Materials Chemistry A **5** (30), 15631 (2017).

[7] C.J. An, Y.H. Kang, H. Song, Y. Jeong, S.Y. Cho, Journal of Materials Chemistry A **5** (30), 15631 (2017).

[8] S.J. Kim, H.E. Lee, H. Choi, Y. Kim, J.H. We, J.S. Shin, K.J. Lee, B.J. Cho, ACS Nano **10** (12), 10851 (2016).

[9] D. Kim, Y. Kim, K. Choi, J.C. Grunlan, C. Yu, ACS Nano **4** (1), 513 (2010).

[10] Q. Yao, L. Chen, W. Zhang, S. Liufu, X. Chen, Acs Nano **4** (4), 2445 (2010).

[11] X.Y. Han, J. Wang, H.F. Cheng, Bulletin of Materials Science **37** (1), 127 (2014).

[12] Y. Cui, K. Wang, B. Wang, Appl. Math. Mech.-Engl. Ed. **39**, 1477 (2018).

[13] W. Wei, J.W. Li, H.T. Zhang, X. M. Cao, C. Tian, J.S. Zhang, Scripta Materialia **57** (12), 1081 (2007).

[14] Y. Ohba, T. Shimozaki, H. Era, Materials transactions **49** (6), 1235 (2008).

[15] C. Zhang, et. al., Ceramics International **41** (7), 9107 (2015).

[16] K. Kim, H. Ju, J. Kim, Composites Science and Technology **123**, 99 (2016).

[17] M. Ohtaki, T. Tsubota, K. Eguchi, H. Arai, Journal of Applied Physics **79**, 1816 (1996).

[18] K.M. Lee, T.Y. Choi, S.K. Lee, D. Poulikakos, Nanotechnology **21** (12), 125301 (2010).

[19] K. Takahashi, et. al., High Temperatures-High Pressures **37** (2), 119 (2008).

[20] L.A. Valentín, J. Betancourt, L.F. Fonseca, M.T. Pettes, L. Shi, M. Soszyński, A. Huczko, Journal of Applied Physics **114** (18), 184301 (2013).

[21] J. Li, et al., Advanced Functional Materials **23** (35), 4317 (2013).

[22] L.D. Zhao, B.P. Zhang, J.F. Li, M. Zhou, W.S. Liu, J. Liu, Journal of Alloys and Compounds **455** (1-2), 259 (2008).

[23] J.F. Li, J. Liu, Physica Status Solidi (a) **203** (15), 3768 (2006).

[24] X.B. Zhao, X.H. Ji, Y.H. Zhang, T.J. Zhu, J.P. Tu, X.B. Zhang, Applied Physics Letters **86** (6), 062111 (2005).

[25] H. Ju, M. Kim, J. Kim, Chemical Engineering Journal **275**, 102 (2015).

[26] L. Zhao, Y. He, H. Zhang, L. Yi, J. Wu, Journal of Alloys and Compounds **768**, 659 (2018).
[27] J. Dong, W. Liu, H. Li, X. Su, X. Tang, C. Uher, Journal of Materials Chemistry A, **1** (40), 12503 (2013).
[28] A. Fissel, B. Schröter, W. Richter, Applied Physics Letters **66** (23), 3182 (1995).
[29] P. Gong, et al., Physics Letters A **382** (35) 2484 (2018).
[30] J.Y. Fan, X.L.Wu, P.Q. Zhao, P.K. Chu, Physics Letters A **360** (2), 336 (2006).
[31] Z.D. Sha, X.M. Wu, L.J. Zhuge, Physics Letters A **355** (3), 228 (2006).
[32] N.F. Andrade, et al., Carbon **90**, 172 (2015).
[33] P.V. Medeiros, et al., ACS Nano **11** (6), 6178 (2017).
[34] X. Wang, K.M. Liew, The Journal of Physical Chemistry C **115** (21), 10388 (2011).
[35] G. Mpourmpakis, G.E. Froudakis, G.P. Lithoxoos, J. Samios, Nano Letters **6** (8), 1581 (2006).
[36] S.H. Barghi, T.T. Tsotsis, M. Sahimi, International Journal of Hydrogen Energy **39** (36), 21107 (2014).
[37] R.S. Singh, A. Solanki, Chemical Physics Letters **660**, 155 (2016).
[38] P.O. Krasnov, F. Ding, A.K. Singh, B.I. Yakobson, J. Phys. Chem. C **111**, 49, 17977 (2007).
[39] W. Zhang, F. Zhang, Z. Zhang, S. Lu, Y. Yang, Science China Physics, Mechanics and Astronomy **53** (9), 1582 (2010).
[40] A. Wu, Q. Song, L. Yang, Q. Hao, Computational and Theoretical Chemistry **977** (1-3), 92 (2011).
[41] M. Mirzaei, M. Mirzaei, Journal of Molecular Structure: THEOCHEM **953** (1-3), 134 (2010).
[42] A. Mahdaviani, M.D. Esrafili, A. Esrafili, Superlattices and Microstructures **60**, 179 (2013).
[43] J. Dai, D. Chen, Q. Li, Physica B: Condensed Matter **447**, 56 (2014).
[44] W. Zhang, F. Zhang, Z. Zhang, S. Lu, Y. Yang, Science China Physics, Mechanics and Astronomy **53** (9), 1582 (2010).
[45] A. Wu, Q. Song, L. Yang, Q. Hao, Computational and Theoretical Chemistry **977** (1-3), 92 (2011).
[46] A.A. Peyghan, H. Soleymanabadi, Z. Bagheri, Journal of the Iranian Chemical Society **12** (6), 1071 (2015).
[47] M. Khodadad, S.M. Baizaee, M. Yuonesi, H. Kahnouji, Physica E: Low-dimensional Systems and Nanostructures **59**, 139 (2014).
[48] S. Choudhary, S. Qureshi, Physics Letters A **375** (38), 3382 (2011).
[49] I. Cabria, M.J. López, J.A. Alonso, The Journal of Chemical Physics **123** (20), 204721 (2005).
[50] P.O. Krasnov, F. Ding, A.K. Singh, B.I. Yakobson, The Journal of Physical Chemistry C **111** (49), 17977 (2007).
[51] T. Yildirim, S. Ciraci, Physical Review Letters **94** (17), 175501 (2005).
[52] E. Masumian, S. M.Hashemianzadeh, A. Nowroozi, Physics Letters A, **378** (34), 2549 (2014).
[53] S. Banerjee, S. Nigam, C.G.S. Pillai, C. Majumder, International Journal of Hydrogen Energy **37** (4), 3733 (2012).
[54] X. Wang, K.M. Liew, The Journal of Physical Chemistry C **115** (8), 3491 (2011).
[55] E. Sjöstedt, L. Nordström, D.J. Singh, Solid State Communications **114** (1), 15 (2000).
[56] N. Troullier, J.L. Martins, Physical Review B **43** (3), 1993 (1991).
[57] K. Schwarz, P. Blaha, G.K.H. Madsen, Computer Physics Communications **147** (1-2), 71 (2002).
[58] J.P. Perdew, et al., Physical Review Letters **100** (13), 136406 (2008).
[59] G.K. Madsen, D.J. Singh, Computer Physics Communications **175** (1), 67 (2006).
[60] S. Behzad, R. Chegel, Solid State Communications **174**, 38 (2013).
[61] M.D. Ganji, N. Seyed-Aghaei, M.M. Taghavi, M. Rezvani, F. Kazempour, Fullerenes, Nanotubes, and Carbon Nanostructures **19** (4), 289 (2011).
[62] S.P. Huang, D.S. Wu, J.M. Hu, H. Zhang, Z. Xie, H. Hu, W.D. Cheng, Optics Express **15** (17), 10947 (2007).
[63] K.J. Li, J.X. Song, H.X. Liu, Advanced Materials Research **625**, 230 (2013).
[64] M. Voeroes, A. Gali, Journal of Computational and Theoretical Nanoscience **9** (11), 1906 (2012).
[65] S. Jiuxu, Y. Yintang, W. Ping, G. Lixin, Z. Zhiyong, Journal of Semiconductors **34** (2), 022001 (2013).